Multiprobe Planar Near-field Range Antenna Measurement System with Improved Performance

Samvel Antonyan[1] and Hovhannes Gomtsyan[1,2]

[1]*National Polytechnic University of Armenia, Yerevan, Armenia,*
[2]*European University of Armenia, Yerevan, Armenia*

https://doi.org/10.26636/jtit.2024.3.1624

Abstract — This article presents a novel multiprobe planar near-field range (PNFR) measurement system. The said system simplifies the overall mechanical design, making it simpler than the existing scanning probe PNFR measurements, and also significantly reduces testing time. A dielectric-based probe is introduced to reduce the antenna size, thereby improving resolution. The probe under consideration is an antipodal Vivaldi antenna offering broadband support and ensuring wideband characteristics of aerials. Numerical results for representative X-band antenna models, presented in the Matlab environment, demonstrate robust performance of the developed measurement system.

Keywords — microstrip patch antenna characteristics, multiprobe PNFR measurements, planar near-field antenna range

1. Introduction

The high degree of complexity associated with antennas operating at high frequencies, resulting from the proportional increase in their far-field, makes standard far-field measurements challenging in open space environments. To avoid these testing difficulties, a near-field antenna measurement technique has been introduced. This technique has gained popularity due to its reduced size and lab footprint.

Despite the fact that near-field measurements are typically performed on a planar, spherical, or cylindrical surface, planar or plane-rectangular near-field measurements are particularly popular due to the simplicity of processing and data acquisition [1]. Assuming that the number of near-field data points is $2^n + 1$, where n is a positive integer, the full plane transformation of the far-field can be computed in a time proportional to:

$$n \cdot a^2 \cdot \log_2(n \cdot a)\,,$$

where a is the radius of the smallest circle in which the test antenna is inscribed [2]. Earlier, other methods, such as bipolar or plane polar near-field measurements, were introduced. Nonetheless, these techniques offer limited benefits when considering the computational cost of the more math-intensive transformation procedure involved [3].

This article proposes a novel technique that leverages multiprobe plane rectangular near-field antenna measurements to improve antenna measurement test time performance and capabilities.

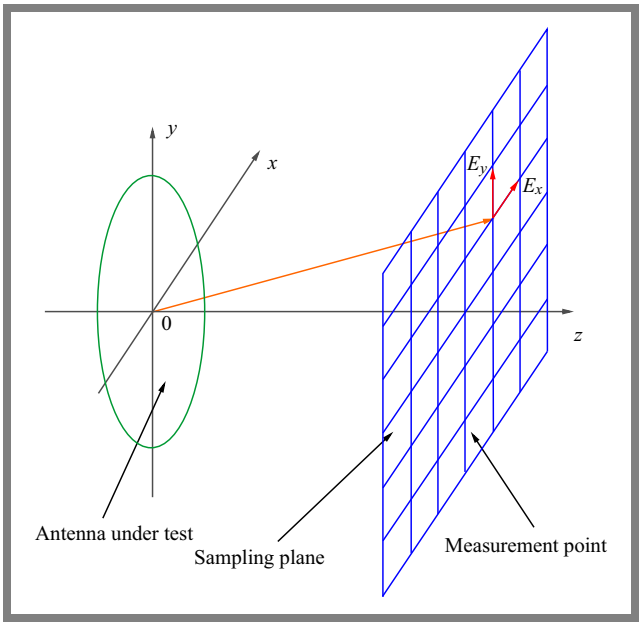

Fig. 1. Planar near-field scanning surface.

2. Problem Statement

In all of the aforementioned cases, acquisition of near field EM vectors is realized by placing the probe at a particular position, pointing it at the direction of the antenna under test (AUT) and allowing the electric field surrounding the probe to generate current. The same procedure should be repeated in two polarizations in order to be able to construct the far-field of the AUT [2]. This technique also refers to "probe scanning", where the probe needs to be moved physically within the specified surface of interest.

Acquisition of planar near-field data is usually conducted over a rectangular $x - y$ grid, as shown in Fig. 1, with a maximum near-field sample spacing of:

$$\Delta x_{max} = \Delta y_{max} = \frac{\lambda}{2}.$$

To ensure near-plane wave measurement conditions at the AUT aperture, the phase taper across the AUT should vary maximum by $\Delta\varphi = \pi/8$ or 22.5° based on its optical analogue, which was proposed in [4]. In practice, this condition can be expressed as:

$$\Delta\varphi(< \frac{\pi}{8}) \approx \frac{\pi D^2}{4\lambda R} , \tag{1}$$

where D is the aperture of the AUT, λ is the operating wavelength, and R is far-field distance.

2.1. Plane Wave (Modal) Expansion

Mathematical formulations of the planar near-field to far-field (NF/FF) system rely on the utilization of plane wave (modal) expansions through Fourier transform techniques. In theory, any form of a monochromatic wave, regardless of its arbitrary nature, can be expressed as a superposition of plane waves propagating in diverse directions, each with distinct amplitudes, but sharing a common frequency.

The primary objective of this plane wave expansion lies in the determination of the unknown amplitudes and propagation directions associated with these constituent plane waves [5]. The relationships between the near-zone E fields and far zone fields for planar systems can be represented by [4]:

$$E_x(x,y,z=0) = \frac{1}{4\pi^2}\iint_{-\infty}^{\infty} f_x(k_x,k_y)e^{-j(k_x x+k_y y)}dk_x dk_y , \tag{2}$$

$$E_y(x,y,z=0) = \frac{1}{4\pi^2}\iint_{-\infty}^{\infty} f_y(k_x,k_y)e^{-j(k_x x+k_y y)}dk_x dk_y , \tag{3}$$

where $f_x(k_x,k_y)$ and $f_x(k_x,k_y)$ represent the plane wave spectrum of the field, x and y are the components of the electric field measured over a plane surface, and k is the wave number. The far field pattern of the antenna, in terms of plane wave spectrum function f, can be found by:

$$E_\theta(r,\theta,\varphi) = j\frac{ke^{-jkr}}{2\pi r}\left(f_x\cos\varphi + f_y\sin\varphi\right) , \tag{4}$$

$$E_\varphi(r,\theta,\varphi) = j\frac{ke^{-jkr}}{2\pi r}\left(-f_x\sin\varphi + f_y\cos\varphi\right) , \tag{5}$$

The generalized methodology for identifying the far field region of an AUT involves several steps. Initially, electric field components are measured in the near field region. Subsequently, the plane wave spectrum functions, denoted as f_x and f_y, are derived by performing a direct inverse fast Fourier transform (FFT) on Eqs. (2) and (3) representing the electric field components. Finally, the far field region is computed by using Eqs. (4) and (5) for the electric field components in spherical coordinates [2].

Although near-field methods are more complicated physically and mathematically, the ability to use small distances means that it is possible to make measurements in a climate-controlled and electromagnetic-controlled environment of an antenna measurement facility, which is not possible in the case of regular far-field measurements. Potentially, this feature can also result in improvements in security, measurement accuracy, and test throughput [6].

In this paper, a multiprobe-based rectangular planar near-field range (PNFR) measurement system, together with an antipodal Vivaldi antenna (AVA)-based near-field probe, is presented. Simulation of the measurement system has been performed with the use of Altair FEKO software, and the near-field to far-field reconstruction has been competed using Matlab.

3. Probe Design

In general, the standard approach to performing a PNFR measurement involves using open-ended waveguides (OEW), as they are quite homogenous in terms of gain across wide frequency ranges. Nevertheless, designing OEWs for higher frequencies can be challenging due to the need to maintain a small footprint to satisfy the $\lambda/2$ sampling point criteria. One of the possible solutions could consists in implementing antennas on dielectrics, which are gaining in popularity these days. The benefit of this approach is that the size of the antenna can be reduced by the ε_r, i.e. the dielectric constant of the substrate [7].

It is also worth noting that one of the other requirements of the PNFR measurement system is that its bandwidth must be sufficient to cover wide frequency ranges. To satisfy all these scenarios, AVA-based near-field probes are designed to be linearly polarized and to operate over a wide bandwidth with high gain [8]. The size of these antennas is quite small due to their dielectric-based substrate. Therefore, they can be easily used in a PNFR lattice. In addition, AVA antennas offer a good return loss and are characterized by minimum signal distortion.

A basic Vivaldi antenna consists of a feed line, usually of the microstrip or stripline type, and the radiating structure. Many Vivaldi antenna designs with different radiating structures have been described in the literature. The exponentially shaped type is the most widely used, as it can provide the broadest band solution [9]. The structure of an AVA antenna is shown in Fig. 2. It includes two main parts, namely the feed line and the radiation flares.

The flares are designed to have the shape of electrical curves, as these configurations provide wide broadband characteristics. The equation for this tapered slot is [9]:

$$y(x) = \pm\left(C_1 e^x + C_2\right) , \tag{6}$$

where C_1 and C_2 are given by:

$$C_1 = \frac{y_2(x) - y_1(x)}{e^{ax_2} - e^{ax_1}} , \tag{7}$$

$$C_2 = \frac{y_1(x)e^{ax_2} - y_2(x)e^{ax_1}}{e^{ax_2} - e^{ax_1}} , \tag{8}$$

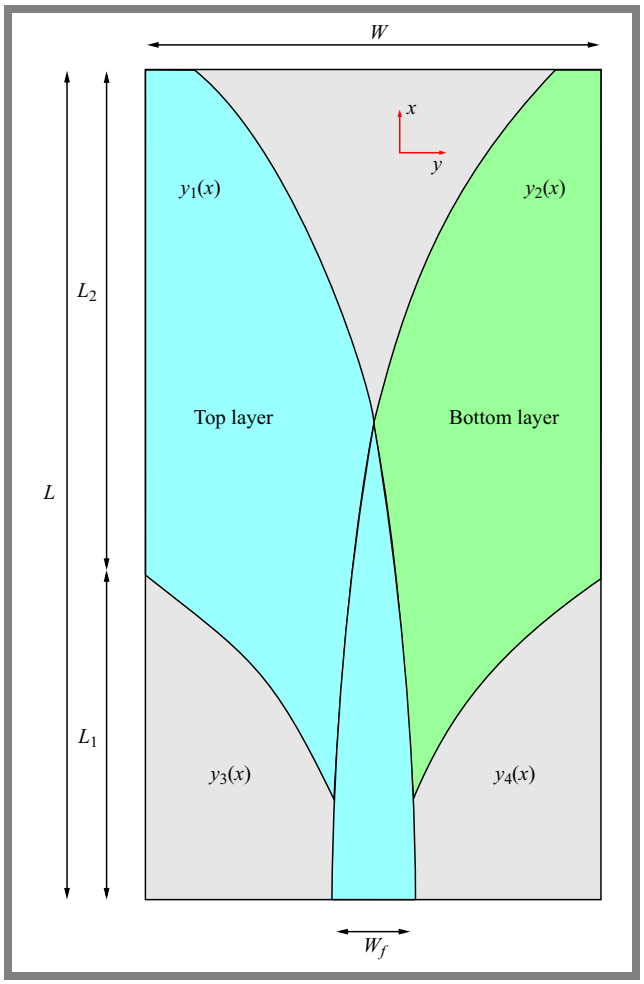

Fig. 2. AVA antenna design.

In these equations, C_1 and C_2 are constants, a is the exponential curve rate, x_1, y_1, x_2, and y_2 are the start and end points of the exponential curve [10] and are defined by:

$$\begin{cases} y_1(x) \rightarrow x_1 = 0, \quad x_2 = L, \quad y_1 = -\dfrac{W_f}{2}, \quad y_2 = \dfrac{W}{2}, \\ y_2(x) \rightarrow x_1 = 0, \quad x_2 = L, \quad y_1 = \dfrac{W_f}{2}, \quad y_2 = -\dfrac{W}{2}, \\ y_3(x) \rightarrow x_1 = 0, \quad x_2 = L_1, \quad y_1 = \dfrac{W_f}{2}, \quad y_2 = \dfrac{W}{2}, \\ y_4(x) \rightarrow x_1 = 0, \quad x_2 = L_1, \quad y_1 = -\dfrac{W_f}{2}, \quad y_2 = \dfrac{W}{2}. \end{cases} \tag{9}$$

The minimum operating frequency range f_{min}, the thickness of substrate h, and its dielectric ε_r constant, as well as length L of the antenna structure are calculated using the following equation [8]:

$$L = \frac{c}{2 f_{min} \sqrt{\varepsilon_{eff}}}, \tag{10}$$

where:

$$\varepsilon_{eff} = \frac{\varepsilon_r + 1}{2} + \frac{\varepsilon_r - 1}{2} \cdot \left(1 + 12 \frac{h}{W}\right), \tag{11}$$

The AVA layout is designed at $f_{min} = 10$ GHz on a substrate with the dielectric constant $\varepsilon_r = 4.6$ and height $h = 10^{-3}$ m. From Eq. (9), the aerial's parameters are: $W = 0.0125$ m, $L = 0.024$ m, $W_f = 2.3 \cdot 10^{-3}$ m for such the line with 50 Ω impedance is achieved.

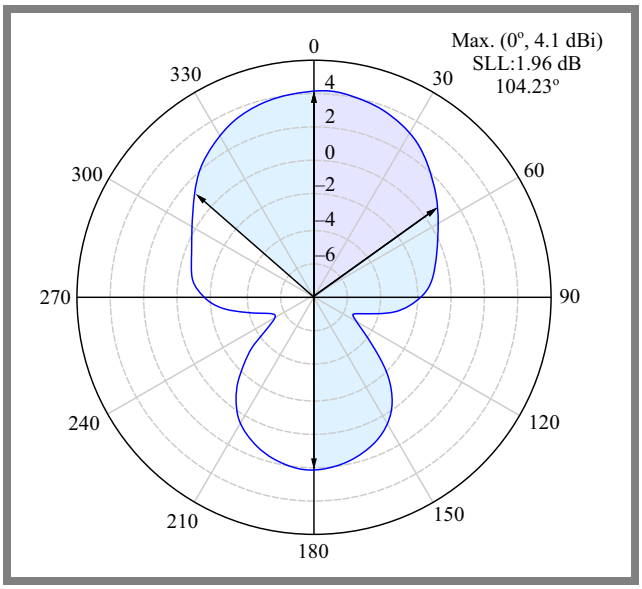

Fig. 3. AVA radiation pattern at 10 GHz in θ plane.

The coefficients of Eq. (9) are obtained during the simulation by optimizing reflection and radiation characteristics. Consequently, the end points of curves $y_3(x)$ and $y_4(x)$ are determined at $L_1 = 9.3 \cdot 10^{-3}$ m, and the equations for top and bottom tapered slots are:

$$\begin{cases} y_1(x) = 17 \cdot 10^{-5}\, e^{150x} - 17 \cdot 10^{-5}, \\ y_2(x) = -\left(17 \cdot 10^{-5}\, e^{150x} - 17 \cdot 10^{-5}\right), \\ y_3(x) = -\left(2 \cdot 10^{-3}\, e^{200x} + 0.3 \cdot 10^{-3}\right), \\ y_4(x) = 2 \cdot 10^{-3}\, e^{200x} + 0.3 \cdot 10^{-3}. \end{cases} \tag{12}$$

As shown in Fig. 3, the beamwidth in θ plane is: $2\,\theta_{0.5}$ =104.23° with a gain of 4.104 dBi.

4. Results and Discussions

The PNFR measurement setup for the operating frequency f_{op} =10 GHz (X-band) was developed with the use of the designed AVA-based near-field probe. A 1×4 phased array antenna is tested as AUT and it is defined in the FEKO environment, for far-field analysis. Results of the design's analysis are then compared with measurements concerning the NF-FF conversion.

4.1. AUT NF Results with PNFR System

As shown in Fig. 4, 17 near field AVA probes have been used in order to create the PNFR measurement setup. The distance between each probe is 3.75 mm, which is sufficient to meet sampling point requirement, as the AUT's operating wavelength is $\lambda_{op}/2$ =14.98 mm >3.75 mm [2]. The AUT is placed at the center of the setup to capture E field data at the $X = 0$ position, where the field strength is assumed to be at its highest value.

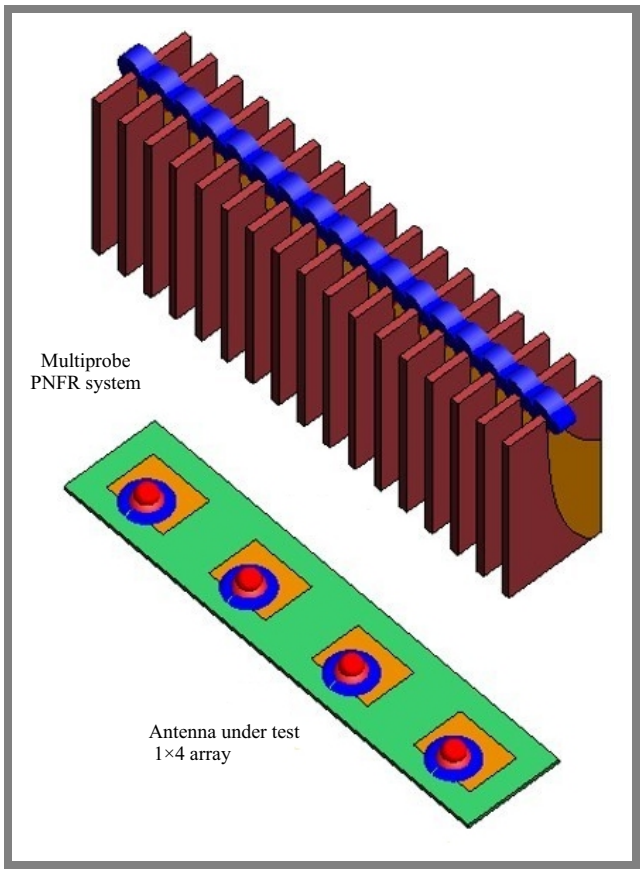

Fig. 4. PNFR measurement system using AVA probes.

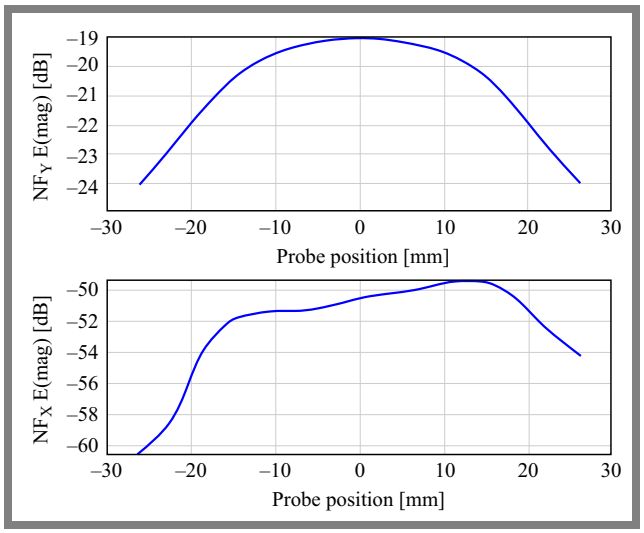

Fig. 5. Measurement results of: a) Ey field and b) Ex field.

The distance between the AUT and the farthest probe is 87.47 mm, which satisfies the radiative near-field distance criteria [6]. To obtain both X and Y polarized electric field components, the AUT was rotated by 90°. The collected E field data is shown in Fig. 5.

4.2. NF–FF Conversion

Resolution of the far-field pattern can be increased by adding artificial data sampling points (with zero value) at the outer extremities of the near-field distribution. This method increases the number of sample points without changing spacing between measurement sample, thus resulting in fixed wavenumber limits. The additional wavenumber spectrum points are within the original wavenumber limits. This leads to increased resolution in the computed far-field patterns [2]. Using the Matlab environment, the plane wave spectrum of both fields is solved by adding artificial data sampling points and applying spline interpolation, as shown in Fig. 6a-b, by using Eqs. (2) and (3).

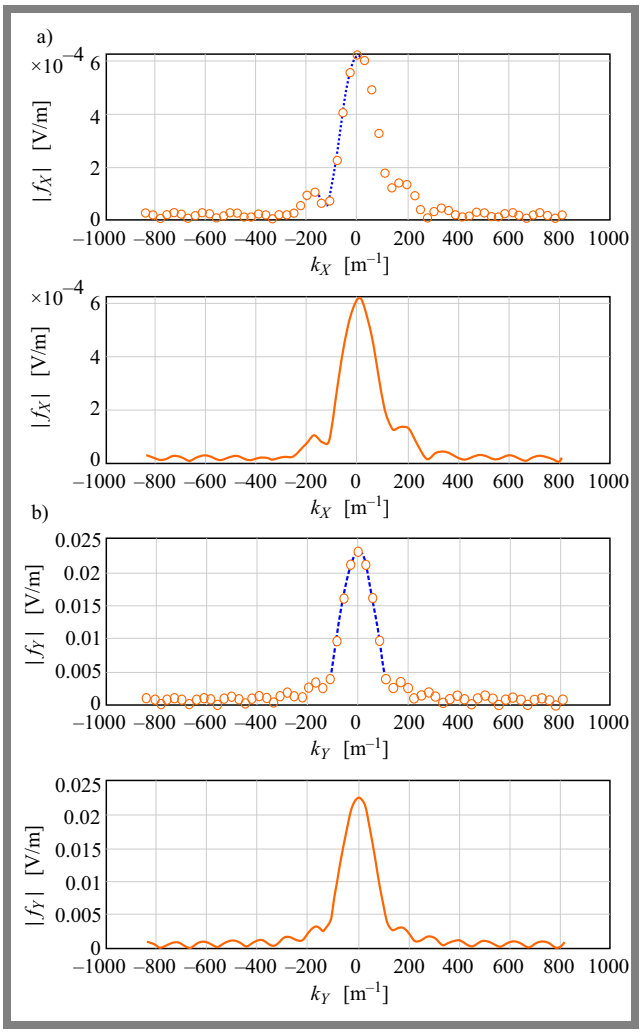

Fig. 6. Interpolated plane wave spectrum for a) x axis and b) y axis.

As mentioned in subsection 2.1, the far-field pattern of the antenna can be determined in terms of plane wave spectrum functions f_x and f_y by using Eqs. (4) and (5). The reconstructed far-field for a 1×4 phased array AUT using such functions is illustrated in Fig. 7. As one may notice, beamwidth in θ plane is $2\,\theta_{0.5} \approx 25.55°$.

4.3. AUT Design Calculation Results with Ideal Scanning Probe Approach

The procedure discussed in subsection 4.1 has been repeated for 51 ideal data sampled results analyzed in the FEKO environment. Based on the gathered dataset, a 2D plot of the analyzed ideal E field is shown in Fig. 8.

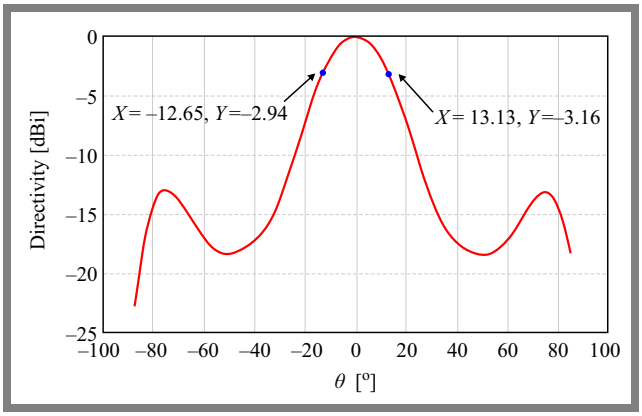

Fig. 7. Reconstructed electric field in θ plane.

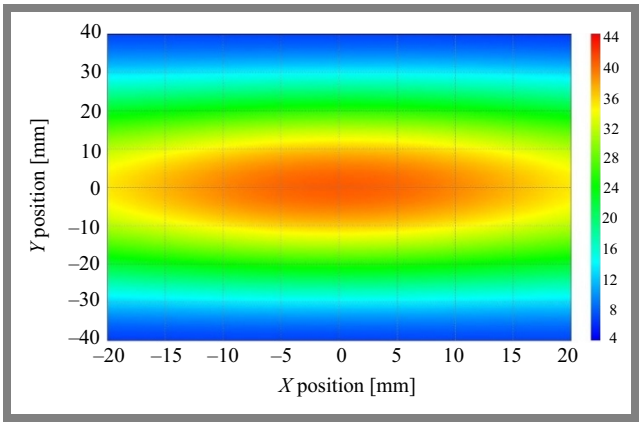

Fig. 8. 2D plot of ideal E in [V/m] in near-field of antenna under test.

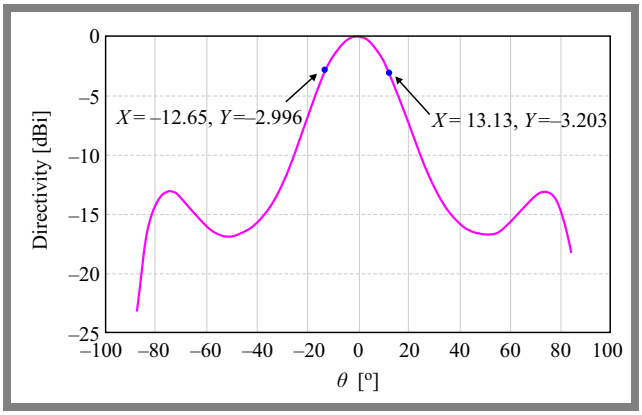

Fig. 9. Reconstructed far-field based on ideal continuous near-field E data in θ plane.

As a result of plane modal expansion and after applying Eqs. (4) and (5), the reconstructed far-field of AUT with the ideal data is shown in Fig. 9.

As one may see, the beamwidth in θ plane equals $2\,\theta'_{0.5} \approx 25.5^\circ$ and is similar to the obtained results, i.e. those that have been reconstructed based on data captured by near-field probes: $\Delta 2\,\theta_{0.5} \approx 2\,\theta_{0.5} - 2\,\theta'_{0.5} \approx 0.05^\circ$.

5. Conclusion

This paper presents the design of a novel multiprobe planar near-field range (PNFR) measurement system, coupled with an antipodal Vivaldi antenna (AVA)-based near-field probe. The multiprobe PNFR system offers a simplified mechanical structure compared to traditional scanning probe methods, leading to significant improvements in terms of testing time and efficiency.

The probe design outlines the process of designing AVA antennas, considering such factors as dielectric substrate properties and geometric configurations to optimize performance. Through simulation and optimization, the AVA antennas demonstrate decent characteristics, including compact size, wide bandwidth, and minimum signal distortion, making them suitable for integration with the PNFR system.

17 dielectric-based AVA probes have been used to characterize a 1×4 phased array as an antenna under test. Near-field probe data of the AUT and ideal near-field data from the FEKO environment were captured for a comparative analysis of AUT's directivity. The captured near-field data was converted to far-field information using an NF-FF reconstruction algorithm implemented in the Matlab environment. Far-field representation of the captured data shows that the difference between the ideal and probe-captured methods is $\Delta 2\,\theta_{0.5} \approx \pm 0.05^\circ$. This small difference proves the validity of the measurement system.

Results from the multiprobe PNFR measurements prove the effectiveness of the system in capturing near-field data with a high degree of precision. Comparison with the ideal scanning probe approach further validates the accuracy and reliability of the multiprobe PNFR method in reconstructing far-field patterns of antennas.

References

[1] A.D. Yaghjian, "An Overview of Near-field Antenna Measurements", *IEEE Transactions on Antennas and Propagation*, vol. 34, no. 1, pp. 30–45, 1986 (https://doi.org/10.1109/TAP.1986.1143727).

[2] C.A. Balanis, *Antenna Theory Analysis and Design*, 3rd ed., John Wiley & Sons, USA, 2005 (ISBN: 9780471667827).

[3] R.G. Yaccarino, Y. Rahmat-Samii, and L.I. Williams, "The Bi-polar Planar Near-field Measurement Technique, Part II: Near-field to Far-field Transformation and Holographic Imaging Methods", *IEEE Transactions on Antennas and Propagation*, vol. 42, no. 2, pp. 196–204, 1994 (https://doi.org/10.1109/8.277213).

[4] S. Gregson, J. McCormick, and C. Parini, *Principles of Planar Near-field Antenna Measurements*, 2nd ed., SciTech Publishing, UK, 634 p., 2023 (ISBN: 9781839536991).

[5] D. Paris, W. Leach, and E. Joy, "Basic Theory of Probe Compensated Near-field Measurements", *IEEE Transactions on Antennas and Propagation*, vol. 26, no. 3, pp. 373–379, 1978 (https://doi.org/10.1109/TAP.1978.1141855).

[6] *IEEE Recommended Practice for Near-Field Antenna Measurements*, IEEE, 2012 (https://doi.org/10.1109/IEEESTD.2012.6375745).

[7] K.E. Kedze, H. Wang, Y.B. Park, and I. Park, "Substrate Dielectric Constant Effects on the Performances of a Metasurface-based Circularly Polarized Microstrip Patch Antenna", *International Journal of Antennas and Propagation*, vol. 2022, art. no. 3026677, 2022 (https://doi.org/10.1155/2022/3026677).

[8] J. Fisher, "Design and Performance Analysis of a 1–40 GHz Ultra-Wideband Antipodal Vivaldi Antenna", *German Radar Symposium GRS 2000*, Berlin, Germany, 2000.

[9] C.B. Hien, H. Shirai, and D.N. Chien, "Analysis and Design of Antipodal Vivaldi Antenna for UWB Applications", *Fifth International Conference on Communications and Electronics (ICCE)*, Danang, Vietnam, 2014 (https://doi.org/10.1109/CCE.2014.6916735).

[10] A.S. Dixit and S. Kumar, "A Survey of Performance Enhancement Techniques of Antipodal Vivaldi Antenna", *IEEE Access*, vol. 8, pp. 45774–45796, 2020 (https://doi.org/10.1109/ACCESS.2020.2977167).

Samvel Antonyan, M.Sc.
Institute of Information and Telecommunication Technologies and Electronics
https://orcid.org/0009-0007-4523-2090
E-mail: samwellantonyan@gmail.com
National Polytechnic University of Armenia, Yerevan, Armenia
https://polytech.am/en/home/

Hovhannes Gomtsyan, Ph.D.
Institute of Information and Telecommunication Technologies and Electronics
https://orcid.org/0009-0003-2479-7923
E-mail: hovhannes.gomcyan@polytechnic.am
National Polytechnic University of Armenia, Yerevan, Armenia
https://polytech.am/en/home/
European University of Armenia, Yerevan, Armenia
https://www.eua.am